Three Dimensional Adhesion Model for Arbitrary Rough Surfaces

S. Deladi, G. Krijnen, N. Tas, M. Elwenspoek

MESA+ Research Institute, University of Twente,
P.O. Box 217, 7500 AE Enschede, The Netherlands
s.deladi@el.utwente.nl

ABSTRACT

We present a 3D adhesion model based on the JKR theory applied locally for all contacting asperity couple and the calculations account the van der Waals interaction beside the externally applied force. Thus, equilibrium of the system is determined by an extremum in the free total energy and subsequently the contact and the adhesion parameters are computed for that particular position. The model estimates the adhesion of contacting arbitrary rough surfaces taking into account that asperities deform according to one of the three deformation regimes (elastic, elasto-plastic and plastic). The deformation of the contacting asperities is determined by the material properties, the asperity characteristics as well as the surface topography. Results show that even outside the bonding regime the specific bonding energy is still high enough to cause adhesive problems for microstructures.

Keywords: adhesion model, surface topography, bonding energy, deformation regime, microstructures.

1 INTRODUCTION

The quick spread of microstructure usage demands an optimised design in order to provide increased reliability. Contacting microstructures generally cease to work properly after a certain period due to the modification of the surface topography caused by adhesion, stiction and friction. The concern about adhesion models has the origin back in the years of sixties when authors studied the behaviour of spherical objects pressed against flat planes and the developed models were mostly built up on the Hertzian contact. Almost at the same time appeared the JKR [4] and the DMT [10] models that later have been included in an adhesion map by Johnson and Williams and the validity of the models was confined. The M-D model [8] represents the transition region between them, but the drawback of all these models is that they can be applied for single asperity contacts and not for arbitrary rough surfaces. Later, authors developed multi-contact models [1,2] including adhesion loads by combining the G-W contact theory [3] or the M-B contact theory for fractal surfaces [9] with one of the single asperity adhesive contact models.

Adhesion has also been investigated by measuring the detachment length of cantilever beams [6] and doubly clamped beams [7] for any particular condition. The importance of predicting the adhesion strength is growing with the complexity of the MEMS devices and the tendency to reduce their dimensions to the lower limit.

2 THE MODEL

The 3D adhesion model is developed on the JKR theory [4], applied locally for each contacting asperity couple. The choice for this particular theory has been determined by the adhesion consideration inside the contact area and the possibility to regard the van der Waals interaction between surfaces when there is no contact as external load applied to the contacting asperities.

The model is applicable for both, computed or measured surfaces. The limitation of the measured surfaces is the convolution effect due to the probing, while for computed surfaces the very spiky asperities must be avoided because of the finite atom radius. This can be achieved by interpolating the three-dimensional surface profile in x and y directions. Computational surfaces can be obtained either by using certain distribution functions if the surface topography parameters are known from previous measurements or by using fractal surfaces. The contacting surfaces can be described then by the functions $z1(x,y)$ and $z2(x,y)$ as shown for example in fig. 1.

The surfaces are divided in finite areas similarly to the meshing for finite element analysis. It has been observed that the adhesion is time dependent and because the time dependence is not known, the incremental approach of the upper surface to the surface below is used. Eq. (1) describes how the position of the surfaces vary with the iteration step:

$$t^{(k)} \rightarrow \begin{cases} z1(x,y)^{(k)} = z1(x,y) \\ z2(x,y)^{(k)} = z2(x,y) - \delta \cdot k \end{cases} \quad (1)$$

where $k = \overline{0..s}$ is the iteration step and _ is the incremental distance. For the sake of not complicating the formulas we will neglect the iteration step indices.

2.1 Forces

Since the weight of the microstructures is usually very small due to the relatively thin layers that can be micro-machined, it can be neglected comparatively to other forces that appear.

When contact occurs between two surfaces the adhesion

lays upon five mechanisms: van der Waals interaction, electrostatic forces, capillary forces, hydrogen bridging and the asperity deformation forces. The model accounts these mechanisms by considering the interfacial energy in the contact regions according to [4].
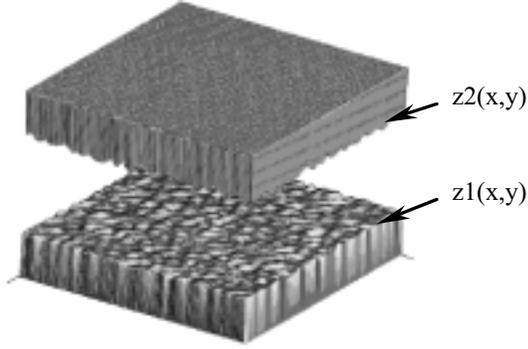

Figure 1: Simulation of two contacting surfaces.

An attractive force will be created outside the contact regions, which can be regarded as an additional term to the externally applied load. Two mechanisms can contribute to this force. Even where there is no contact but the surfaces are in close proximity the van der Waals interaction plays an important role and the force due to this mechanism is:

$$Fw = \begin{cases} \sum_{i=1}^{n-1} \sum_{j=1}^{n-1} \dfrac{H\,A_{i,j}}{6\pi\,d_{i,j}^3} & if\ z2(x,y) > z1(x,y) \\ 0 & otherwise \end{cases} \quad (2)$$

$$A_{i,j} = (x_{i+1} - x_i)(y_{j+1} - y_j)\ i = \overline{1..n-1}, j = \overline{1..m-1}$$

$$d_{i,j} = z2\left(\frac{x_{i+1}+x_i}{2}, \frac{y_{j+1}+y_j}{2}\right) - z1\left(\frac{x_{i+1}+x_i}{2}, \frac{y_{j+1}+y_j}{2}\right)$$

where H is the Hamaker constant, d is the mean value of the distance between finite areas.

Charging can occur accidentally or by purpose between surfaces, while the normal forces for MEMS devices are mostly created by electrostatic attraction:

$$Fe = \begin{cases} \sum_{i=1}^{n-1} \sum_{j=1}^{n-1} \dfrac{\varepsilon\,A_{i,j}U^2}{2(d_{i,j} + t_{i,j})^2} & if\ z2(x,y) > z1(x,y) \\ \sum_{i=1}^{n-1} \sum_{j=1}^{n-1} \dfrac{\varepsilon\,A_{i,j}U^2}{2 t_{i,j}^2} & otherwise \end{cases} \quad (3)$$

where t is the thickness of the insulator layer (typically 0.5-1 _m) and U is the applied voltage.

The model can account for mechanically applied loads Fm by simply adding it to the normal load.

Then, the total normal load F that must be distributed on the contacting asperities is obtained by the summation of Fw, Fe and Fm.

2.2 Computational ground

Analysing the sign function defined by eq. (4) the contact areas and the non-contact areas can be separated like in fig. 2. The computations showed that is important to take into account the three-dimensional asperity shapes and positions because the tilt angle _ between the planes defined by the perimeters of the interferences and the horizontal plane can vary up to 10-11 degrees (fig. 3).

$$S = sign[\,z2(x_i, y_j) - z1(x_i, y_j)\,] \quad (4)$$
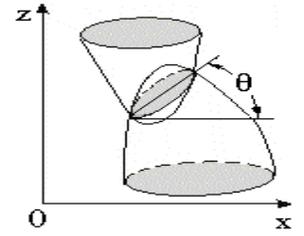

Figure 2: Area separation.   Figure 3: Tilt angle _.

In the regions where the surface profiles would theoretically interfere, the dimensions of the areas determined by the perimeters of the interferences are computed in x and y directions and then used for substituting the asperities with spherical cap shaped ones. The radii of the base planes of the spherical caps rc will be equal to half of the mean value of those dimensions. The distance between the centre point of the base plane and the value of the profile function for the x and y coordinates of the centre point determines the height δc of each spherical cap. The radius of the spherical cap can be determined by forcing a circle to pass through three points of its cross section.

Having the radii of the contacting asperities for both surfaces we have the possibility to apply the JKR adhesive model for the asperity couples. In order to simplify the algorithm and to gain computation speed, the contacting asperities have been renumbered and thus vectors have been used in further calculations instead of matrixes. The composite radii for all p asperity couples will be:

$$R_i = \frac{R(z1)_i R(z2)_i}{R(z1)_i + R(z2)_i} \quad i = \overline{1..p}\,. \quad (5)$$

Due to the finite compliance of the matter and random distribution of the asperities the total normal load must be distributed according to their geometrical characteristics:

$$F_i = F\frac{\left(3rc_i^2 + \delta c_i^2\right)\delta c_i^2}{\sum_{i=1}^{p}\left(3rc_i^2 + \delta c_i^2\right)\delta c_i^2} \quad (6)$$

where rc and $\_c$ are defined above.

The apparent contact load for the contacting asperities due to the interfacial energy can be obtained by modifying the JKR formula [4] for the apparent contact load:

$$Fa_i = F_i \cos\theta_i + 3\pi\Gamma R_i + \sqrt{6\pi\Gamma R_i F_i \cos\theta_i + (3\pi\Gamma R_i)^2} \ . \quad (7)$$

The equilibrium position of the surfaces can be determined with the free total energy Et of the system eq. (8), which consists of the mechanical energy Em of the normal loads, the surface energy Es and the stored elastic energy Ee.

$$Et = Em + Es - Ee \qquad (8)$$

Some of the previous multi-contact model reports [1,2,3] considered elastic deformation of the asperities and defined the limitation of the models using the plasticity index. Due to different sizes of the contacting asperities the plasticity index of each contacting asperity couple will be different as follows:

$$\varphi_i = \frac{E}{Ha}\left(\frac{\sigma}{R_i}\right) \quad i = \overline{1..p} \qquad (9)$$

$$\frac{1}{E} = \frac{1-v1^2}{E1} + \frac{1-v2^2}{E2}; \ \ \sigma = \left(\sigma 1^2 + \sigma 2^2\right)^{1/2}$$

where σ is the composite standard deviation, E is the composite elasticity modulus and Ha is the hardness of the softer material.

The authors propose a way to include all three deformation regimes, namely the elastic deformation regime $\varphi \le 0.6$, the fully plastic deformation regime $\varphi > 1.1$ and the intermediate regime (elasto-plastic). It can be observed that the stored elastic energy accounts for all three deformation regimes, eq. (10.2).

$$Em = \sum_{i=1}^{p} \frac{F_i \cos\theta_i}{R_i^{\frac{1}{3}} K^{\frac{2}{3}}} \left[\frac{1}{3}\left(Fa_i \cos\theta_i\right)^{\frac{2}{3}} + \frac{2}{3}\left(F_i \cos\theta_i\right)\left(Fa_i \cos\theta_i\right)^{\frac{-1}{3}}\right]$$

$$Es = \pi\Gamma \sum_{i=1}^{p} rc_i^2 \ ; \ \ K = \frac{4}{3}E \qquad (10.1)$$

The iteration stops when the incremental free total energy becomes zero and the adhesive contact parameters can be calculated such as the real contact area, the pull-off force and the modified surface topography. Generalising the pull-off force of the single asperity adhesive contact and adding the van der Waals force because this must also be over-

come, will give us the pull-off force of the plates, eq. (11).

$$Fp = -\frac{3}{2}\Gamma\pi \sum_{i=1}^{p} R_i - Fw \qquad (11)$$

The topography of the surfaces modifies due to the deformation of the asperities in plastic and intermediate regimes (fig. 5). Returning to the numbering system of the finite areas, a matrix of plasticity index must be constructed in order to allow the computation of the modified surfaces. The plasticity index matrix is built up with nil elements where there is no contact and the subsequent plasticity index for each contacting asperity in the region where they are placed. Considering the hardness of the contacting materials, two cases must be defined: (1) if the hardness of the materials are nearly the same $a \cdot H1 \le H2 \le H1/a$, then the deformation of the surface profiles is according to eq. (12) with deformations in all three regimes; (2) if not, then the harder material will deform the softer one according to eq. (13). The real contact area is calculated by addition of the finite surfaces where the modified surface profiles would touch each other at equilibrium (fig. 4).

$$z1 = \begin{cases} z1 & \text{if } (z1 \le z2) \vee (z1 > z2 \wedge \phi \le 0.6) \\ z1 - 2P(\phi - 0.6) & \text{if } z1 > z2 \wedge \phi \in (0.6,1.1) \\ z1 - P & \text{if } z1 > z2 \wedge \phi \ge 1.1 \end{cases} \qquad (12)$$

$$z1 = \begin{cases} z1 & \text{if } (z1 \le z2) \vee (z1 > z2 \wedge a \cdot H1 > H2) \\ z2 & \text{if } z1 > z2 \wedge a \cdot H2 > H1 \end{cases} \qquad (13)$$

$$P = \frac{z1 - z2}{4\left[1 - \frac{\ln(H2/H1)}{\ln(a)}sgn\left(\ln\frac{H2}{H1}\right)\right]}sgn\left(\ln\frac{H2}{H1}\right) + \frac{z1 - z2}{2}$$

The modified surface profile of the upper surface is calculated with similar considerations. Notice that a is usually in the range of 0.9-0.95 and it depends on the place of the contacting materials on the Mohr scale.

3 RESULTS

Because a large part of the contacts for MEMS devices is represented by the polysilicon-polysilicon contact and because silicon wafer bonding is of high importance, contact between two silicon plates has been simulated and the results have been compared with a previous model and experiments [2]. Figure 4 shows the importance of the interfacial energy in establishing the equilibrium position of the plates.

A cross section view of the surface profile before and after

$$Ee = \sum_{i=1}^{p} \frac{1}{K^{2/3}} \frac{1}{R_i^{1/3}} \left[\frac{1}{15}\left(Fa_i \cos\theta_i\right)^{\frac{5}{3}} + \frac{1}{3}\left(F_i \cos\theta_i\right)^2\left(Fa_i \cos\theta_i\right)^{\frac{-1}{3}}\right] \cdot \begin{cases} 1 & \text{if } \varphi_i < 0.6 \\ 1 - 2(\varphi_i - 0.6) & \text{if } 0.6 \le \varphi_i \le 1.1 \\ 0 & \text{if } \varphi_i > 1.1 \end{cases} \qquad (10.2)$$

pull-off (fig. 5) proves that not all the asperities deform in the same regime and the deformation is depending on the characteristics of each asperity.
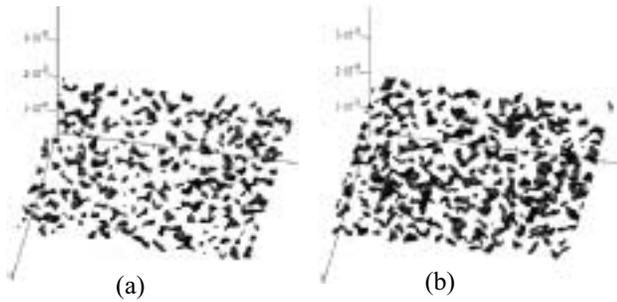

(a)   (b)

Figure 4: Contact interfaces for (a) _ = 1; (b) _ = 2.8.

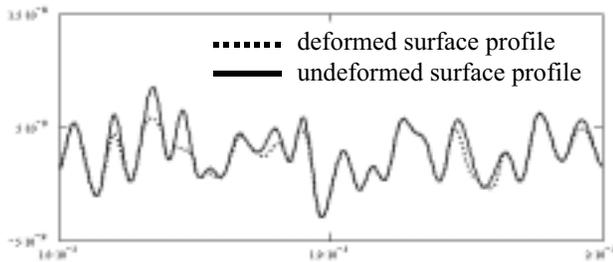....... deformed surface profile
—— undeformed surface profile

Figure 5: Topography modification.

A mean value of the adhesion parameter _ has been considered in order to allow a comparison with other models:

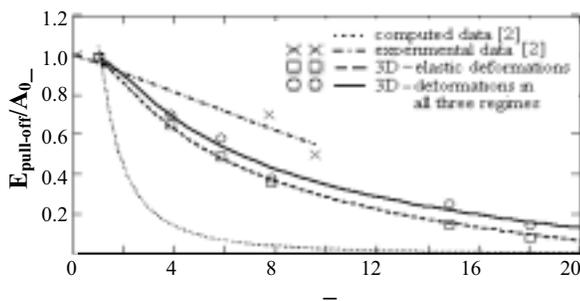$$\theta = \frac{1}{p}\sum_{i=1}^{p}\frac{E}{\Gamma}\sqrt{\frac{\sigma^3}{R_i}} \quad . \tag{14}$$

Figure 6: Normalized bonding energy variation.

The results presented in fig. 6 show that even outside the bonding regime $è < 1$, the specific bonding energy is still high enough to cause adhesive problems for microstructures. If some asperities deform plastically or according to the intermediate region, then the iteration stops few steps later relative to the case when only elastic deformations occur due to the stored elastic energy

diminution. Thus, the real surface area as well as the pull-off force will increase as one can see in fig. 6,7.
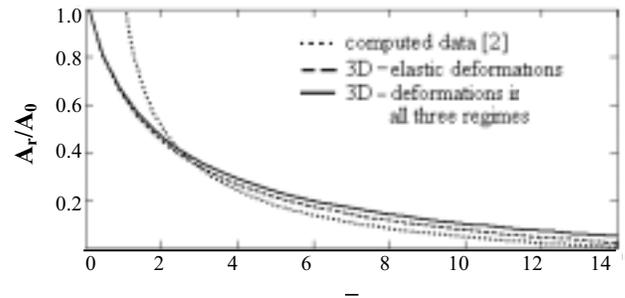

Figure 7: Normalized contact area variation.

For very rough surfaces the van der Waals interaction is weak due to large separation distances between the subsequent finite areas.

CONCLUSIONS

We have presented a numerical model that is capable of successfully estimating adhesive forces between two arbitrary surfaces taking into account van der Waals forces, normal forces, elastic and plastic deformation of the contacting asperities.

The topography modification is a consequence of the interaction between asperities and it is guided by the material properties and the topography parameters.

The van der Waals interaction can be strong when the surfaces are not in touch but in close proximity. Some asperities will deform plastically even if external loads are not applied.

If there are asperities that do not deform elastically, then the real contact area will be larger and the pull-off force will be higher than in the case of only elastic deformations.

Even outside the bonding regime the specific bonding energy is still high enough to cause adhesive problems for microstructures.

The model can also serve as a ground for static friction study at micro/nanoscale between surfaces.

REFERENCES

[1] Chang, W.R., et al., J. of Tribology 110, 1988, 50.
[2] Gui, C., et.al., J. App. Physics 85(10), 1999, 7448.
[3] Greenwood, J.A., Williamson, J.B.P, Proc. Roy. Soc. London Series A295, 1966, 300.
[4] Johnson, K.L., et al., Proc. Roy. Soc. London Series A324, 1971, 301.
[5] Komvopoulus, K., Wear, 200, 1996, 305.
[6] De Boer, M.P., et.al., Acta Materialia 48(18-19), 2000, 4531.
[7] Legtenberg, R., et.al., Sensors and Act. A43, 1994, 230.
[8] Maugis, D., J. Colloid Interface Sci. 150, 1992, 243.
[9] Majumdar, A., Bhushan, B., J. of Trib. 113, 1991, 1.
[10] Derjagin, B.V., et.al., J. Coll. Int. Sci. 67, 1978, 378.